Electrochemical Behaviors of Binary and Ternary Manganese Phosphides

F. Gillot,[†] L. Monconduit,*[,‡] and M.-L. Doublet*[,§]

LRCS-CNRS 7002 Université de Picardie Jules Verne, 33, rue St Leu, F80039 Amiens Cedex, France and LAMMI-CNRS 5072 Université Montpellier II and LSDSMS-CNRS 5636 Université Montpellier II, Place E. Bataillon, F34095 Montpellier Cedex 5, France

Received June 10, 2005. Revised Manuscript Received September 5, 2005

The present work provides a comparative study of the electrochemical behaviors of binary and ternary manganese phosphides toward lithium. The redox mechanism involved in these two electrodes is elucidated by means of galvanostatic and in situ X-ray diffraction measurements and first-principles calculations. Compared to the previous study reported on MnP_4, two additional processes are here clearly identified: after a first conversion process that transforms the binary MnP_4 electrode into Li_7MnP_4, a partial and irreversible decomposition of Li_7MnP_4 into $Li_3P + Mn^0$ is achieved, responsible for the poor electrodes capacity retention. In charge, the formation of an amorphous low-lithiated $Li_{\sim 1}MnP_4$ phase, very similar to the charged Li_xVP_4 and Li_xTiP_4 electrodes ever reported, is shown to compete with the kinetically limited MnP_4 reconstruction. This suggests that the high performances of ternary transition metal phosphides could be combined with the technological advantage of using more suitable nonlithiated MP_4 starting anodes.

1. Introduction

Preferred negative electrode materials for lithium-ion batteries are carbonaceous materials in various forms (coke, graphitic carbons, etc.).[1,2] Alternatives to commercial carbonaceous materials are highly sought to overcome the limitations of low gravimetric and volumetric capacity and safety concerns that these materials exhibit. Active/inactive alloys formed by tin, antimony, aluminum, and silicon exhibit capacity fading and poor gravimetric capacity and require difficult techniques of preparation.[3−5] Main group oxides (Sn) and transition metal oxides exhibit high polarization, large irreversible capacity, and capacity fading.[6,7] Transition metal nitrides also show capacity fading, but above all they are difficult to synthesize and lead to moisture-sensitive products that cannot be prepared without lithium.[8,9] Recently, ternary transition metal phosphides Li_xMP_4 (M = Ti, V)[10−12] were proposed as interesting materials, showing high gravimetric capacities (up to 1000 $mAhg^{-1}$) in their first charge and discharge cycles, with flat voltage profiles around 1 volt. These performances were correlated to a strong structural stability of the $(MP_4)^{x-}$ tetrahedral entities toward large charge variations (up to 10 Li), leading to small electrode volume expansions upon cycling.[11,13] Nevertheless, most of these materials suffer from insufficient capacity retentions and all of them present implementing issues regarding common anodic applications: they have to be first "charged" to extract lithium. To meet the remarkable structural and electrochemical properties of the ternary Li_xMP_4 cubic systems with the technological advantages provided by the use of binary nonlithiated transition metal phosphides, we and others investigated a new class of nano- to microstructured binary transition metal phosphides M_xP_y (M = Ti, V, Cr, Mn, Fe, Co, Ni, Cu, Zn).[14] Among these materials, Cu_3P shows very encouraging results and a better cycling life than the ternary Li_xMP_4 phases.[15−17] FeP_2 also presents a high capacity in first discharge but a poor capacity retention.[14,18]

* Authors to whom correspondence should be addressed. E-mail: moncondu@univ-montp2.fr; doublet@univ-montp2.fr.
[†] LRCS-CNRS 7002 Université de Picardie Jules Verne.
[‡] LAMMI-CNRS 5072 Université Montpellier II.
[§] LSDSMS-CNRS 5636 Université Montpellier II.

(1) Yazami, R. *J. Power Sources* **2001**, *97*, 33.
(2) Cao, F.; Barsukov, I. V.; Bang, H. J.; Zaleski, P.; Pratkash, J. *J. Electrochem. Soc.* **2000**, *147*, 3579.
(3) Kepler, K. D.; Vaughey, J. T.; Thackeray, M. M. *Electrochem. Solid-State Lett.* **1999**, *2*, 307.
(4) Song, S.-W.; Striebel, K. A.; Reade, R. P.; Robert, G. A.; Cairns, E. J. *J. Electrochem. Soc.* **2003**, *150*, A121.
(5) Aldon, L.; Garcia, A.; Olivier-Fourcade, J.; Jumas, J. C.; Fernandez-Madrigal, F. J.; Lavela, P.; Pérez Vicente, C.; Tirado, J. L. *J. Power Sources* **2003**, *119*, 585.
(6) Idota, Y.; Kubota, T.; Matsujuji, A.; Maekawa, Y.; Miyasaka, T. *Sciences* **1997**, *276*, 570.
(7) Courtney, I. A.; Dahn, J. R. *J. Electrochem. Soc.* **1997**, *144*, 2943.
(8) Pereira, N.; Klein, L. C.; Amatucci, G. G. *J. Electrochem. Soc.* **2002**, *149*, A262.
(9) Shodai, T.; Okada, S.; Tobishima, S.; Yamaki, J. *J. Power Sources* **1997**, *68*, 515.
(10) Doublet, M.-L.; Lemoigno, F.; Gillot, F.; Monconduit, L. *Chem. Mater.* **2002**, *14*, 4126.
(11) Bichat, M.-P.; Gillot, F.; Monconduit, L.; Favier, F.; Morcrette, M.; Lemoigno, F.; Doublet, M.-L. *Chem. Mater.* **2004**, *16*, 1002.
(12) Gillot, F.; Bichat, M.-P.; Favier, F.; Morcrette, M.; Doublet, M.-L.; Monconduit, L. *Electrochim. Acta* **2004**, *47*, 3137.
(13) Doublet, M.-L.; Lemoigno, F.; Bichat, M.-P.; Favier, F.; Monconduit, L. *Proceeding of the 204th Meeting of the Electrochemical Society*, Orlando, 2004.
(14) Boyanov, S.; Gillot, F.; Monconduit, L.; Doublet, M.-L. To be published, 2005.
(15) Bichat, M.-P.; Politova, T.; Pascal, J.-L.; Favier, F.; Monconduit, L. *J. Electrochem. Soc.* **2004**, *151*, A2074.
(16) Crosnier, O.; Nazar, L. F. *Electrochem. Solid-State Lett.* **2004**, *7*, A187.
(17) Mauvernay, B.; Bichat, M.-B.; Favier, F.; Morcrette, M.; Monconduit, L.; Doublet, M.-L. *Ionics* **2005**, *11*, 39.
(18) Silva, D. C. C.; Crosnier, O.; Ouvrard, G.; Greedan, J.; Safa-Sefat, A.; Nazar, L. F. *Electrochem. Solid-State Lett.* **2003**, *6*, A162.

10.1021/cm051245j CCC: $30.25
Published on Web 10/14/2005

More recently, the TiP_2 compound synthesized by ball-milling method was shown to exhibit high capacity (~900 $mAhg^{-1}$) retained after 10 cycles.[19]

In this paper, we focus on the Li/Mn/P system, providing a comparative study of the electrochemical behaviors of the ternary Li_7MnP_4 and the binary MnP_4 materials, both synthesized by high-temperature routes. Li_7MnP_4 has a cubic structure ($Fm\bar{3}m$) built on nearly isolated MnP_4 tetrahedra[20] while MnP_4 has a monoclinic ($C2/c$) structure built on edge-shared MnP_6 octahedra.[21] In a recent work, Nazar and co-workers[22] showed that the MnP_4 electrode undergoes a reversible solid state (crystalline) transformation associated with the reaction $MnP_4 + 7{*}Li \leftrightarrow Li_7MnP_4$. This structural transition was claimed to be perfectly reversible, on the basis of galvanostatic intermittent titration (GITT) experiments showing nearly equivalent equilibrium potentials in oxidation (1.06 V) and in reduction (1.03 V). A significant capacity fading is nevertheless observed during the first charge which stabilizes only after 50 cycles, leading to dramatic capacity fading for this MnP_4 electrode. In a previous work, we showed that starting from the ternary cubic Li_7MnP_4 phase obtained through ball-milling synthesis, MnP_4 is never identified on charge, whatever the potential window used for the measurements, up to 2.0−0.0 V.[23,24] Instead, the electrode follows the same voltage profile as those previously reported for the homologous Li_xMP_4 (M = Ti, V) phases.[10−13] This raises the question of the reversibility of the $MnP_4 + 7{*}Li \leftrightarrow Li_7MnP_4$ reaction. One possible explanation for these different behaviors could lie in the electrode morphologies since different synthetic routes were used to prepare both the binary (high temperature) and the ternary manganese phosphides (ball-milling), resulting in different crystallite sizes. As extensively shown by previous studies,[25−27] the use of ball-milling methods for the electrode preparation significantly decreases the particles size of the reaction products, leading to nearly amorphous electrode associated with better specific capacity and cycling life. To make the comparison valuable between the binary MnP_4 and the ternary Li_7MnP_4 systems, it was therefore necessary to set free the particles size effect on the electrode electrochemical performances. For sake of comparison with the previous study reported by Nazar and co-workers,[22] Li_7MnP_4 and MnP_4 were synthesized by close ceramic methods, to obtain products with equivalent powder morphologies.

2. Results

(a) Synthesis and Characterization. The binary MnP_4 phase can be prepared under high-pressure conditions, but also by a tin-flux method, as reported in ref 22. Manganese powders, red phosphorus, and tin powder were mixed (Mn:P:Sn equal to 1:10:6) in a quartz tube that was evacuated and sealed. The tube was heated at 600 °C for 3 weeks and air-quenched. The powder was rinsed with an aqueous solution of HCl (1:1). The obtained MnP_4 powder is air-stable. This tin-flux method gives rise to highly crystallized MnP_4 powder with particles size varying from 1 to 100 μm.[28] The ternary Li_7MnP_4 phase was synthesized from the elements into stainless steel tubes sealed under argon by arc welding. Stoichiometric amounts of Li, Mn, and red phosphorus (99%, Aldrich) were heated at 900 °C for 20 h and quenched in air to prevent the formation of stable Li_3P binary phases. Starting materials and products are air- and moisture-sensitive and were handled in an argon-filled glovebox (O_2 and H_2O below 5 ppm). The Li_7MnP_4 sample also presents nicely crystallized particles with averaged size from 10 to 100 μm.[28] This is at least 1 order of magnitude larger than the particles size previously obtained for Li_7MnP_4 using a ball-milling process[24] but suitable for a proper comparison with MnP_4.

The XRD patterns collected for the two systems are consistent with the monoclinic lattice of MnP_4 ($C2/c$ space group; $a = 10.513$ Å, $b = 5.0940$ Å, $c = 21.804$ Å, $\beta = 94.71$[21]) and with the cubic lattice of Li_7MnP_4 ($Fm\bar{3}m$ space group; $a = 5.9770$ Å[20]). The structure of MnP_4 is described by tetramers of edge-shared octahedra linked to each other by P−P bridges to form a two-dimensional network of interconnected zigzag chains, in the (b,c) plane. As shown in Figures 1a and 1b, this tetramer packing forms a layered-type structure with short interlayer P−P distances (2.27 Å), preventing any lithium insertion. The structure of Li_7MnP_4 is described by nearly isolated MnP_4 tetrahedra (see Figure 1c), as extensively discussed in our previous work on ternary transition metal pnictides.[10−13,24]

(b) Electrochemical Properties. Electrochemical lithium insertion/extraction tests were performed in Swagelok-type cells assembled in an argon-filled drybox, with oxygen and water contents below 5 ppm. These cells consist of a composite electrode containing 10−12 mg of active material mixed with 15% of acetylene black as positive electrode, a lithium metal disk as negative electrode, and a Whattman GF/D borosilicate glass microfiber separator saturated with 1 M $LiPF_6$ (EC:DMC, 1:1) electrolyte solution (Merck S.A) placed in between. The electrochemical insertion was monitored either using a VMP automatic cycling/data recording system (Biologic SA) or a Mac Pile (Biologic SA) in the range 1.7 to 0.5 V and 2.0 to 0.01 V operating in galvanostatic or potentiodynamic modes, at a 1 Li/15 h scan rate.

The voltage−composition and potentiodynamic curves obtained for the MnP_4 electrode,[28] started in discharge between 1.7 and 0.5 V at a 1 Li/15 h rate, are similar to

(19) Woo, S.; Sohn, H.-J. Abs. 264, IMLB 12 Meeting, The Electrochemical Society, 2004.
(20) Juza, R.; Bohmann, T. *Z. Anorg. Allg. Chem.* **1961**, *308*, 159.
(21) Jeitschko, W.; Donohue, P. C. *Acta Crystallogr., Sect. B* **1975**, *31*, 574.
(22) Souza, D. C. S.; Pralong, V.; Jacobson, A. J.; Nazar, L. F. *Science* **2002**, *296*, 2012.
(23) Gillot, F. Ph.D. Thesis, Université Montpellier, 2003.
(24) Gillot, F.; Monconduit, L.; Morcrette, M.; Doublet, M.-L.; Tarascon, J.-M. *Chem. Mater.* **2005**, ASAP.
(25) Morcrette, M.; Gillot, F.; Monconduit, L.; Tarascon, J.-M. *Electrochem. Solid-State Lett.* **2003**, *6*, A59.
(26) Larcher, D.; Masquelier, C.; Bonnin, D.; Chabre, Y.; Masson, V.; Leriche, J.-B.; Tarascon, J.-M. *J. Electrochem. Soc.* **2003**, *150*, A133.
(27) Rougier, A.; Soiron, S.; Haihal, I.; Aymard, L.; Taouk, B.; Tarascon, J.-M. *Powder Technol.* **2002**, *128*, 139.

(28) XRD patterns and SEM images of both MnP_4 and Li_7MnP_4 preparations are provided as Supporting Information.

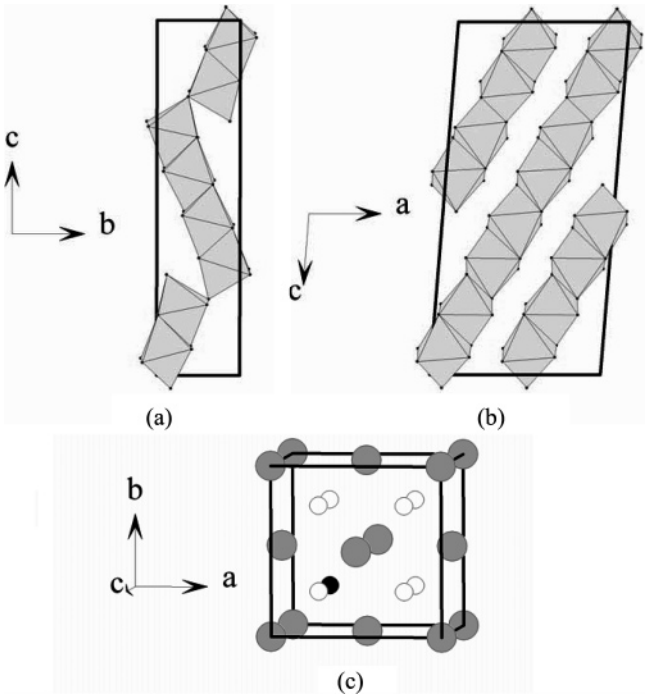

Figure 1. MnP_6 octahedra packing in the crystal structure of MnP_4 projected along the *a*-axis (a) and *b*-axis (b). Crystal structure of the Li_7MnP_4 (c) in which Li, Mn, and P atoms are illustrated by white, black, and gray circles.

those previously reported by Nazar et al. using an equivalent potential window and provided as Supporting Information.[22] Under such conditions, a large plateau is observed at 0.62 V that confirms a two-phase reaction. This first process is ended when almost 7 lithium ions are inserted into the electrode, in agreement with the decomposition reaction $MnP_4 + 7^*Li \rightarrow Li_7MnP_4$. The consecutive charge reaches a lithium composition of $x = 2.5$, which corresponds to one-third of capacity loss compared to the discharge. The second discharge does not follow the voltage plateau characteristic of the MnP_4 to Li_7MnP_4 crystalline phase transition observed in the first discharge. It is characterized by a sloppy potential curve and by a dramatic capacity fading, as for the consecutive charges and discharges. As shown in Figure 2a, one more process is observed when the MnP_4 electrode is discharged down to 0.01 V, compared to 0.5 V, resulting in a very poor capacity retention. It is characterized in Figure 2b by a rather large incremental peak of capacity around 0.2 V. This process corresponds to the insertion of almost three more lithium, leading to the "$Li_{9.5}MnP_4$" electrode and could be associated, at first sight, with a SEI layer formation. Surprisingly, the occurrence of this low-voltage process seems to have no influence on the charge process, as lithium extraction clearly proceeds in two steps whatever the potential window applied. A simple comparison of the potential values and shapes for these two processes in charge would be sufficient to state they correspond to the same reactions. They occur at 1.22 and 1.50 for the MnP_4 electrode charged from 0.5 to 1.7 V and at 1.20 and 1.56 V for the MnP_4 electrode charged from 0.01 to 2.0 V. This indicates that forward (discharge) and back (charge) reactions involve different mechanisms and not one unique and reversible process as previously reported by Nazar et al.[22] During the second discharge, the thin incremental peak of capacity

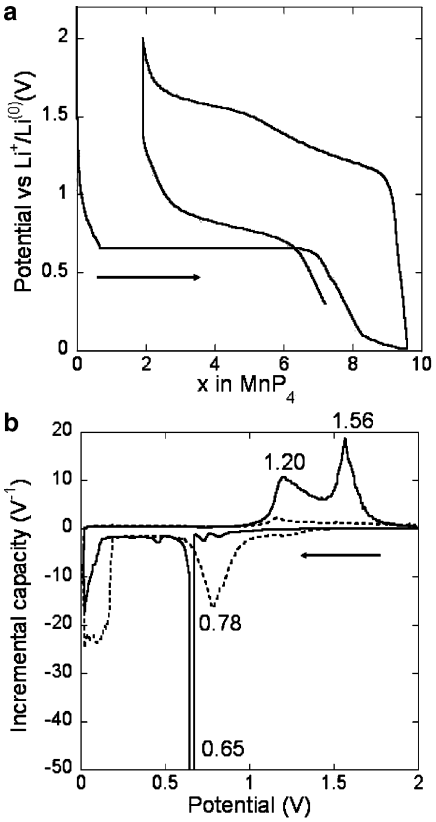

Figure 2. (a) Voltage−composition profile and (b) derivative d*x*/d*V* for the MnP_4/Li cell, at 1 Li/15 h in the 0.01−2.0 V potential window. The solid and dotted lines refer to first and second cycles, respectively.

associated with the initial decomposition reaction $MnP_4 + 7^*Li \rightarrow Li_7MnP_4$ is replaced by a broader peak at 0.75 and 0.78 V for the two electrodes, respectively. The second low-voltage process observed during the first discharge around 0.2 V is still observed during the second discharge.

The voltage−composition curve obtained for Li_7MnP_4 (started in charge) between 2.0 and 0.01 V at a 1 Li/15 h rate is presented in Figure 3a. The general shape of this curve is very close to that obtained for MnP_4 after the first discharge. As for the MnP_4 electrode, charge does not proceed down to $x = 0$, suggesting that all lithium cannot be extracted from the Li_7MnP_4 to form MnP_4. This is corroborated by the derivative d*x*/d*V* curve of Figure 3b that shows incremental peaks of capacity at 1.22 and 1.5 V upon charge and at 0.74 and 0.17 V upon discharge. An even larger capacity loss than for MnP_4 has to be deplored for this electrode, supporting the irreversible decomposition of Li_7MnP_4 into $Li_3P + Mn^0$.

(c) In Situ X-ray Diffraction (XRD). To correlate the redox processes to the electrode structural behaviors, in situ XRD patterns were collected during discharge/charge for the MnP_4/Li and Li_7MnP_4/Li cells in the full potential window, using a D8 Brucker X-ray diffractometer with Co Kα radiation. The in situ electrochemical cell was mounted in a drybox by placing the studied electrode material underneath a beryllium window used as current collector, the electrochemical active part of the cell being the same as that in our Swagelok configuration. The complete device was then placed in the diffractometer and connected to the VMP cycling system. As shown in Figure 4a, the reflections of

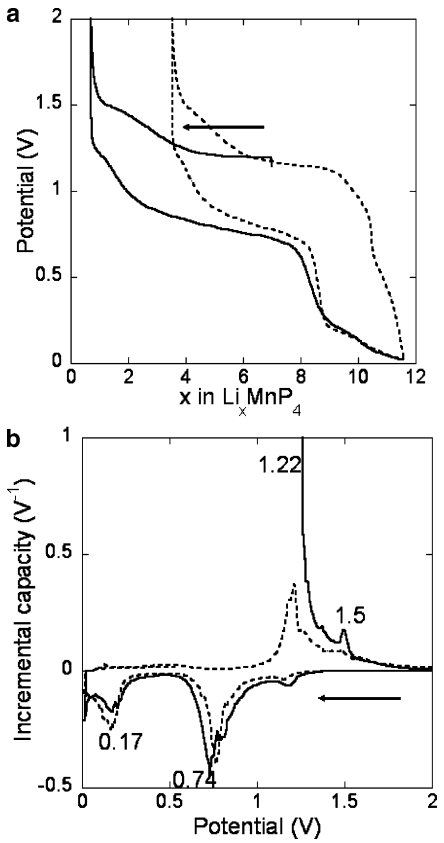

Figure 3. (a) Voltage−composition profile and (b) derivative dx/dV for the Li_7MnP_4/ Li cell, at 1 Li/15 h in the 0.01−2.0 V potential window. The solid and dotted lines refer to first and second cycles, respectively.

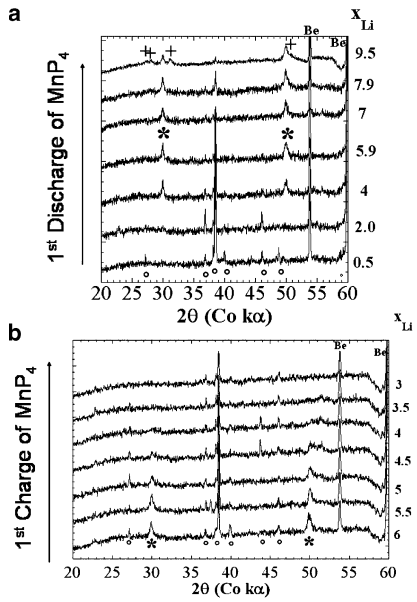

Figure 4. In situ X-ray (Co Kα_1) diffraction patterns collected at various first cycle states of the MnP_4/Li electrochemical cell, (a) during the first discharge and (b) the first charge. The characteristic peaks of Li_7MnP_4 (stars), MnP_4 (open circles), and Li_3P (crosses) are represented for sake of clarity.

the starting MnP_4 material rapidly decrease during the first discharge of MnP_4/Li, but are still evident at $x = 7$. Meanwhile, the characteristic peaks of the Li_7MnP_4 cubic phase progressively grow ((111) and (220) Bragg peak, at $2\theta = 30°$ and 50°, respectively). The two-phase reaction $MnP_4 + 7{*}Li \rightarrow Li_7MnP_4$ is thus confirmed even though it is incomplete, probably due to the large particles size resulting in low kinetics. From $x = 7.9$ to $x = 10$ the characteristic peaks of Li_7MnP_4 decrease without any Bragg angles displacement, suggesting a two-phase process. As clearly identified in Figure 4a, the decrease of Li_7MnP_4 is linked with the growth of the hexagonal Li_3P phase ((100) at $2\theta = 28°$, (101) at $2\theta = 31°$, and (110) and (103) at $2\theta = 50°$). A conversion reaction is thus expected to take place in the second part of the discharge, leading to the decomposition of Li_7MnP_4 into Li_3P and Mn^0, although no evidence of Mn^0 could be found in the in situ XRD patterns. As for the first reaction, this second reaction is incomplete since 5 Li would be required to fully achieve the $Li_7MnP_4 + 5{*}Li \rightarrow 4{*}Li_3P + Mn^0$ transformation. It should also be noticed that the residual peaks of MnP_4 are still identified at the end of discharge ($x = 9.5$), suggesting that MnP_4 is not involved in the second reaction (cf. Figure 4a).

On charge, the (111) and (220) characteristic peaks of the Li_7MnP_4 cubic phase are first shifted down to higher angles, suggesting a single- or two-phase process associated with the formation of a less-lithiated phase exhibiting a contracted cubic cell parameter (see Figure 4b). These peaks then progressively vanish down to lithium composition close to $x = 3$. In this second part of charge, the MnP_4 characteristic peaks suddenly increase. These two successive reactions suggest that MnP_4 is not reformed directly from Li_7MnP_4, but from a contracted cubic phase of lower lithium composition. A reversible phase transition would have implied no displacement in the Bragg angles of the Li_7MnP_4 characteristic peaks and a concomitant growing of the MnP_4 characteristic peaks. The nucleation delay of the MnP_4 will be discussed in the next section.

An in situ X-ray diffraction Li_7MnP_4/Li cell was also assembled and charged up to 2 V before being discharged down to 0.01 V. As for MnP_4, the charge corresponds to a progressive shift of the (111) and (220) toward higher 2θ angles, together with a decrease in the peak intensity (Figure 5a). For x values reaching 2, the XRD powder patterns become featureless, indicative of a total X-rays amorphous phase and remain the same up to the end of charge. The fully charged electrode of composition "$Li_{1.3}MnP_4$" is amorphous. The electrochemical lithiation of the fully oxidized "$Li_{1.3}MnP_4$" electrode (Figure 5b) leads to the reappearance of the cubic phase ((111) and (220) Bragg peaks). These peaks continuously grow until a lithium composition close to $x = 7$, showing that the electrode has converted back to its initial crystallized cubic structure. Further pursuing the electrochemical lithiation of Li_7MnP_4 by lowering the cell voltage down to 0.01 V results in a progressive decrease of the (111) and (220) Bragg peaks intensity, together with a progressive growth of two extra Bragg peaks located at $2\theta = 31°$ and 50° corresponding to the formation of Li_3P. As previously noticed for MnP_4, the Mn^0 characteristic peaks are not evident in the XRD patterns at the end of discharge. This suggests that nanosized metallic particles are embedded in a Li_3P matrix, as previously corroborated by high-resolution transmission electronic

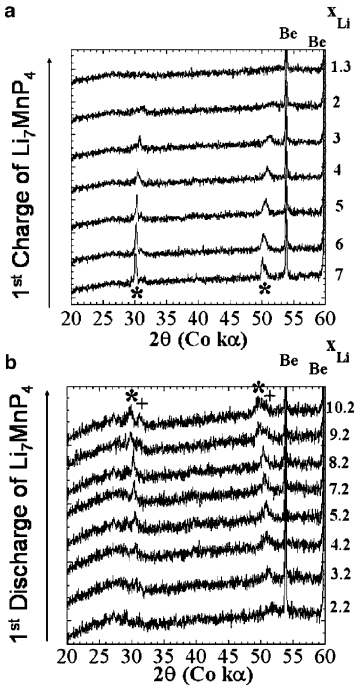

Figure 5. In situ X-ray (Co $K\alpha_1$) diffraction patterns collected at various first cycle states of the Li_7MnP_4/Li electrochemical cell, (a) during the first charge and (b) the first discharge. The characteristic peaks of Li_7MnP_4 (stars) and Li_3P (crosses) are represented for sake of clarity.

microscopy (HRTEM) using a small electron probe less than 100 Å. [24] Moreover, as observed for MnP_4, the transformation of Li_7MnP_4 into Li_3P and Mn^0 is incomplete since peaks of the ternary phase are still evident at the end of discharge (Figure 4a).

3. Redox Mechanism

(a) Discharge. Both MnP_4 and Li_7MnP_4 electrodes have nearly equivalent electrochemical behaviors once the first discharge of MnP_4 is achieved. The $MnP_4 + 7^*Li \rightarrow Li_7MnP_4$ crystalline phase transition previously demonstrated by Nazar and co-workers is confirmed here. The process characterized in the first discharge of MnP_4 by the incremental peak at 0.62 V is clearly associated by in situ XRD with a transformation of the monoclinic MnP_4 binary phase into the cubic Li_7MnP_4 ternary phase. This is supported by first-principles density functional theory (DFT) calculations, using the VASP code developed by Haffner et al.[29] Full structural relaxations and total energy calculations show a very good agreement between the computed[30] and the experimental potentials for the $MnP_4 + 7^*Li \rightarrow Li_7MnP_4$ reaction and the unit cell parameters relaxed for the two acting phases (see Table 1). This first reaction is however not fully accomplished due to kinetic effects since the MnP_4 product powder consists of large particles size, even larger than that obtained by Nazar and co-workers using the same synthesis route (<0.1 μm).[22] A second reaction associated with an incremental peak of capacity close to 0.2 V is shown to take place in the second part of the discharge for both MnP_4 and Li_7MnP_4 electrodes. This process, which has not been reported yet corresponds to an incomplete decomposition reaction of Li_7MnP_4 into Li_3P and Mn^0. Kinetic and/or morphological factors could be at the origin of such reaction incompletion. On one side, the large electrode particle size may obviously avoid efficient lithium diffusion into the electrode, and the important structural rearrangements associated with the decomposition of Li_7MnP_4 into $Li_3P + Mn^0$ may result in electrode cracking.

Table 1. Electrochemical potentials calculated for different two-phase reactions using the method proposed by Ceder et al. in ref 30; relaxed unit cell parameters for MnP_4, Li_5MnP_4, and Li_7MnP_4 and Mn−P bond orders (integrated crystal orbital overlap population (ICOOP)) in Li_5MnP_4 and Li_7MnP_4

	experimental (V)	computed (V)	Mn−P ICOOP
$MnP_4 + 7^*Li \rightarrow Li_7MnP_4$	$V_{exp} = 0.62$	$-\Delta G/nF = 0.637$	
$Li_7MnP_4 \rightarrow Li_5MnP_4 + 2^*Li$	$V_{exp} \sim 1.50$	$-\Delta G/nF = 1.594$	
MnP_4 crystal structure	$a = 10.513$ Å	$a = 10.519$ Å	
	$b = 5.094$ Å	$b = 5.097$ Å	
	$c = 21.804$ Å	$c = 21.778$ Å	
	$\beta = 94.71°$	$\beta = 94.59°$	
Li_7MnP_4 crystal structure	$a = 5.977$ Å	$A = 5.874$ Å	0.61
Li_5MnP_4 crystal structure	$a < 5.977$ Å	$a = 5.778$ Å	0.63

The structural changes associated with the electrochemical insertion of 7 Li in MnP_4 to form Li_7MnP_4 can be directly correlated to the local electronic structure of Mn in both an octahedral (MnP_4) and a tetrahedral (Li_7MnP_4) environment. To illustrate this point, we performed molecular electronic structure calculations using the CAESAR code[31] based on the extended Hückel tight-binding method (EHTB). As shown in Figure 6, the splitting of the manganese 3d orbitals in an octahedral environment leads to one block of empty phosphorus-like levels (namely, the P-type molecular orbitals) lying between the metallic-like levels (namely, the t_{2g}-type and e_g-type molecular orbitals). This leads to the half-filling of the metallic t_{2g}-type orbitals and to the metallic electronic configuration d^3 (Figure 6a). In a tetrahedral environment, the splitting of the manganese 3d orbitals leads to one low-lying block of fully filled P-type orbitals and two high-lying blocks of metallic-like orbitals, namely, the e-type and the t_2-type molecular orbitals. Compared to the octahedral environment, this is now the e-type orbitals which are half-filled, thus leading to a metallic electronic configuration d^2 (Figure 6b). This means that the insertion of 7 electrons (and $7Li^+$) into the MnP_4 electrode corresponds to an increase of the manganese oxidation state, showing that the redox center involved in the $MnP_4 + 7^*Li$ reaction is not the transition metal but primarily the phosphorus. Since each of the t_{2g}-type and P-type orbitals correspond to strong antibonding Mn−P and P−P interactions, respectively, it is straightforward to see that filling the local $(MnP_6)^{2-}$ electronic structure with 7 electrons will contribute to Mn−P and P−P bonds destabilization. This results in the breaking of the P−P bridges occurring in the MnP_4 structure along with the reduction of P and the formation of $(MnP_4)^{7-}$

(29) Kresser, G.; Hafner, J. *Phys. Rev. B* **1993**, *47*, 558.
(30) Aydinol, M. K.; Kohan, A. F.; Ceder, G.; Cho, K.; Joannopoulos, J. *Phys. Rev. B* **1997**, *56*, 1354.
(31) The molecular electronic structure calculations were carried out using the CAESAR program package developed by Ren, J.; Liang, W.; Whangbo, M.-H. Crystal Electronic Structure Analysis Using CAESAR. http://www.primeC.com, 1998.

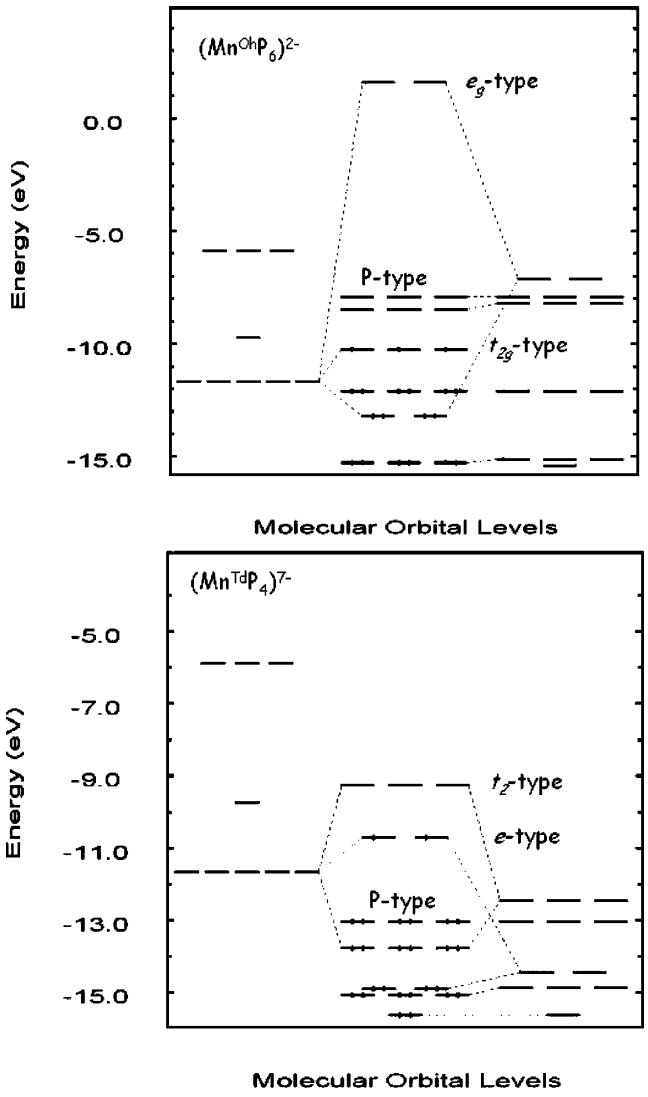

Figure 6. EHTB electronic structures for (a) the octahedron $(MnP_6)^{2-}$ and (b) the tetrahedron $(MnP_4)^{7-}$ calculated using the CAESAR program package.

tetrahedra. The reasons why this reaction is a two-phase reaction originate from one structural and one electronic factor: (i) there is no available space for lithium in the MnP_4 monoclinic structure, and (ii) the manganese is known to behave as a strongly correlated transition metal, for which half-filled (high-spin) electronic configurations are often preferred to other fractional ones. It should be noticed here that even though covalent Mn−P bonds occur in these systems, spin-polarized calculations confirm the high-spin density around the transition metal. This metallic feature should also be at the origin of the second two-phase reaction occurring at the end of discharge, and leading to the partial formation of Li_3P and Mn^0. Indeed, the manganese extruded from the Li_7MnP_4 structure keeps a stable half-filled electronic configuration, i.e., Mn^0 (d^5). Compared to the first reaction for which phosphorus atoms were the redox centers, the second reaction mainly involves the manganese as the redox center. It is interesting to note that this second two-phase reaction is unable to take place in early transition metal phosphides, as both Li_5TiP_3 and Li_7VP_4 electronic structures lead to a metallic electronic configuration d^0, thus avoiding the complete filling of the e-type and t_2-type orbitals and therefore the complete M−P destabilization, whatever the lithium composition reached at the end of discharge.

(b) Charge. Whatever the potential window used for the MnP_4/Li and Li_7MnP_4 cells, i.e., allowing or preventing the second decomposition reaction, two equivalent processes occur in charge for the two electrodes. This strongly suggests that the low-potential decomposition reaction is irreversible, supporting the poor capacity retention observed for the two electrodes. Similar decomposition reactions were observed in 3d transition metal oxides,[32] or in ternary borates,[33] in which the electrochemical reaction toward Li leads to the formation of Li_2O matrix embedding metallic particles. While for oxides the reversible reaction has been clearly identified, it was shown to be avoided by the presence of other decomposition products in the discharged borate electrodes. In the present case of strongly covalent Mn−P systems, this decomposition reaction seems to be irreversible since significantly better capacity retention is achieved for the Li_7MnP_4 electrode when the potential window avoids its decomposition into $Mn^0 + Li_3P$.[24] The strong cohesive energy of the metallic Mn^0 bulk could be at the origin of this irreversibility, as it is one of the largest among the first-row transition metals. The free energy associated with the formation of Mn nanoparticles is then expected to be highly negative, leading to high-energy barriers for the reversible reaction. Moreover, this back reaction corresponds to the preparation reaction of the whole series of ternary transition metal pnictides Li_xMPn_4, which is known to be achievable under high-temperature and/or high-pressure[20] conditions only. Even if the thermodynamic point of view cannot be solely considered here, and that the nanosized nature of Li_3P and Mn^0 should obviously result in large surface contributions which could help in lowering the back reaction energy barrier, our experimental results tend to support that Li_7MnP_4 is not reformed from the $Li_3P + Mn^0$ electrodes.

The two different processes characterized in charge for both the Li_7MnP_4 and the MnP_4 starting electrodes and occurring at very close potentials thus suggest similar behaviors for the two systems. Equivalent in situ XRD signatures are obtained for the first process, suggesting that Li_7MnP_4 transforms into a slightly contracted cubic phase of lithium composition close to $x = 5$. It is difficult here to state whether this first process corresponds to a solid solution or a two-phase reaction since very close in situ XRD patterns are expected in both cases. More accurate X-rays collections would be required to reach better peak definitions and to address this question. Be that as it may, the previously mentioned correlated feature of manganese would be more consistent with a two-phase reaction. Indeed, as shown by the total and projected DOS of Figure 7, two different redox bands are involved in charge, starting from the Li_7MnP_4 electrode. For this composition, the Fermi level lies in a high-lying metallic band that describes π-type (e-type) antibonding Mn−P levels. The low-lying and fully occupied band describes P-type nonbonding levels and Mn−P bonding

(32) Dedryvere, R. Laruelle, S.; Grugeon, S.; Poizot, P.; Gonbeau, D.; Tarascon, J.-M. *Chem. Mater*. **2004**, *16*, 1056.
(33) Patoux, S.; Vannier, R.-N.; Mairesse, G.; Nowogrocki, G.; Tarascon, J.-M. *Chem. Mater*. **2001**, *13*, 500.

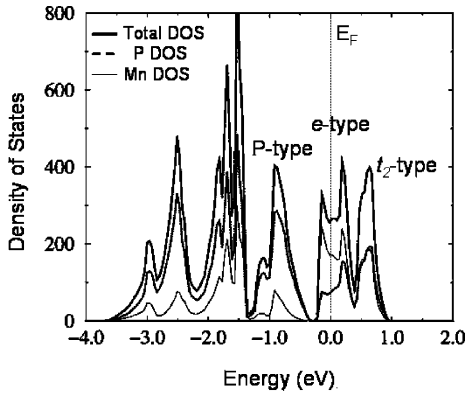

Figure 7. Total (thick solid) and projected density of states on both Mn (thin solid) and P (dashed) computed for the fully relaxed Li_7MnP_4 structure. The vertical dotted line stands for the Fermi level.

levels. Since a partial occupation of the e-type band is not favorable in the case of strongly correlated systems, it is most likely that a two-phase reaction takes place between Li_7MnP_4 and Li_5MnP_4. This hypothesis is supported by first-principles electronic structure calculations and structural relaxations performed on Li_5MnP_4, showing a good agreement with both the computed potential of the two-phase reaction and the contraction of the unit cell parameter for the low-lithiated phase (see Table 1).

For $x \leq 5$, the general shape of the MnP_4 and Li_7MnP_4 voltage profiles in charge resembles that of the previously reported Li_xMP_4 (M = Ti,V) electrodes.[10−13] In these latter systems, charge was shown to occur through one process, transforming the high-lithiated crystallized electrode into a low-lithiated X-rays amorphous electrode. The entropy gain associated with the formation of a Li-disordered and P-disordered (loss of *fcc* reflections) low-lithiated phase was put forward as the driving force of this reaction. In the present case, the oxidation of the Li_5MnP_4 electrode into the MnP_4 initial structure requires both short-range and long-range structural rearrangements: (i) Mn−P bonds have to be modified to recover the manganese octahedral environment starting from the tetrahedral environment, and (ii) P−P bridges have to be reformed to allow the large reoxidization of the phosphides. Obviously such structural rearrangements imply high-energy barriers and should strongly depend on the electrode morphology and on the charge rate. In MnP_4, the shortest Mn−Mn distance is 2.943 Å while it is least twice this distance in Li_5MnP_4 (i.e., the cubic cell parameter). Even if different forms of less packed MnP_6 octahedra exist for MnP_4, the MnP_4 reconstruction should be kinetically limited by the diffusion of large MnP_4 anionic species, as confirmed by the rather strong covalent character of the Mn−P bonds in the cubic Li_5MnP_4 and Li_7MnP_4 phases (see the ICOOP bond orders in Table 1). Moreover, the occurrence of inactive Li_3P and Mn^0 in the electrode should also contribute to this limited diffusion. Hence, unless the MnP_4 nucleation is facilitated by the presence of MnP_4 germs in the electrode, a more facile electrode amorphization should be preferred. The structural mechanism associated with this amorphization corresponds to a contraction of the $(MnP_4)^{x-}$ tetrahedral entities in order to compensate for the lack of cationic charge around and is facilitated by the strong ability of the electron density to rearrange on covalent Mn−P bonds.[11]

Concluding Remarks

The present work shows that binary and ternary manganese phosphides exhibit a more complex redox behavior than the previously reported early transition metal phosphides Li_5TiP_3, Li_7VP_4, and Li_9VAs_4. This has been directly linked to the nature and to the electronic configuration of manganese compared to those of titanium and vanadium. After a first lithiation that transforms MnP_4 into Li_7MnP_4, very similar electrochemical behaviors are observed for both the binary and the ternary starting electrodes, in the successive discharges and charges. This suggests that the Li_7MnP_4 prepared through high-temperature synthesis is very close to that obtained through a redox chemistry process from the binary MnP_4. The poor electrodes cycling life has been correlated to the partial and irreversible conversion of Li_7MnP_4 into Li_3P and Mn^0 at the end of discharge. In charge, a first process associated with the formation of a ternary Li_5MnP_4 contracted cubic phase has been characterized by in situ XRD for the two electrodes and confirmed by first-principles structural relaxations. A direct MnP_4 reconstruction from Li_7MnP_4 through the reversible first-order solid-state transition $MnP_4 + 7^*Li \leftrightarrow Li_7MnP_4$ previously proposed by Nazar et al. is here kinetically limited and is shown to compete with the more facile electrode amorphization, already described in other transition metal phosphides. Morphological, structural, and electronic factors can be at the origin of this competition: (i) the occurrence of inactive Li_3P and nanosized Mn^0 particles in the electrode preventing the diffusion of the large covalent $(MnP_4)^{x-}$ species required for the MnP_4 nucleation, (ii) the averaged Mn−Mn distance occurring in the Li_7MnP_4 electrode which is probably different depending on its preparation mode, i.e., redox chemistry or high temperature, and (iii) the reoxidation of the stable low-lying and fully reduced phosphides.

Despite the poor capacity retention obtained for both the binary and the ternary electrodes, the present results are encouraging as they allow meeting the remarkable structural and redox mechanism of the ternary $Li_xM_yPn_4$ cubic systems with the technological advantages provided by the use of binary nonlithiated and air-stable starting electrodes. To increase the electrochemical performances of MnP_4, we have undertaken the synthesis of nanosized MnP_4 powders especially to improve the kinetics and to decrease the capacity loss associated with the irreversible Li_7MnP_4 to Li_3P and Mn^0 transformation. X-ray absorption spectroscopy (XANES, EXAFS) was also planned to characterize the intermediate Li_5MnP_4 phase.

Acknowledgment. L.M. thanks the SAFT company for its financial support. The authors thank J.-M. Tarascon for helpful discussions and technical support.

Supporting Information Available: Two additional figures showing X-ray diffraction patterns, voltage−composition profiles, and potentiodynamic curves. This material is available free of charge via the Internet at http://pubs.acs.org.

CM051245J